ELSEVIER

Journal of Molecular Catalysis A: Chemical 131 (1998) 209–224

JOURNAL OF MOLECULAR CATALYSIS A: CHEMICAL

The use of normal mode calculations to interpret reflection absorption infrared spectra of molecular adsorbates

P. Mills [1], D. Jentz [2], M. Trenary *

Department of Chemistry, University of Illinois at Chicago, 845 W. Taylor Street, Chicago, IL 60607-7061, USA

Received 13 June 1997; accepted 5 August 1997

Abstract

Normal mode calculations were used to analyze the infrared spectra of a number of novel adsorbates possessing iminium-($C{=}NH_2$) like functionalities, which are formed from a variety of precursor molecules containing the CN moiety on Pt(111). Calculations confirm that aminomethylidyne (CNH_2) is generated from methylamine (CH_3NH_2) and low coverages of hydrogen cyanide (HCN), while diaminoethylene ($H_2NC{=}CNH_2$) is formed through the hydrogenation of cyanogen (C_2N_2). It is also shown that CNH_2 dimers are formed via the thermal decomposition of either azomethane ($CH_3N_2CH_3$) or $(CNH_2)_2$, as well as through the aggregation of CNH_2 formed from high HCN exposures. © 1998 Elsevier Science B.V.

Keywords: Reflection absorption infrared spectra; Molecular adsorbate; Pt(111)

1. Introduction

Surface vibrational spectroscopy is widely used to determine the identity and structure of molecular adsorbates [1]. This use parallels the more general application of infrared and Raman spectroscopy in which a great deal of qualitative information is provided from the symmetry selection rules and spectral assignments based on the concept of group frequencies [2]. A more quantitative interpretation of vibrational spectra is almost universally based on the normal mode description of the vibrational degrees of freedom [3]. An understanding of spectral features that are outside the normal mode framework is generally based on the assumption of weak perturbations of the normal modes. Within the normal mode description, a more fundamental way of characterizing the information obtained from a set of vibrational data is to determine the harmonic force field. The harmonic force field is obtained from the experimental data through a normal mode analysis. In addition to providing an experimental force field, a normal mode analysis can provide useful insights into the internal structure and bonding of molecular species. While normal mode analyses have been used since the very beginning of vibrational spectroscopy, they have not been widely used in

* Corresponding author. E-mail: mtrenary@uic.edu

[1] Present address: Department of Chemistry, Cambridge University, Lensfield Road, Cambridge, CB2 IEW, UK.

[2] Present address: Intel Corporation, 5200 N.E. Elam Young Parkway, Hillsboro, OR 97124-6497, USA.

PII S1381-1169(97)00267-7

the interpretation of surface vibrational spectra. In this paper we describe in detail the application of normal mode calculations to interpret reflection absorption infrared (RAIR) spectra of a series of molecular adsorbates on Pt(111).

While a variety of coordinate systems can be used in a normal mode analysis, force fields obtained in terms of internal coordinates, such as bond stretching and bond bending, offer the greatest physical insight into the internal bonding of a molecule. A simple illustrative example is provided by the 'CN stretch' fundamentals of HCN and FCN, which occur at 2097 and 2290 cm^{-1}, respectively [2]. Based on the frequencies alone, one might (erroneously) conclude that FCN has a 'stiffer' CN bond. Although the CN stretch force constants are very similar for the two molecules, HCN actually has the higher value [4,5]. In this case the composition of the two stretching normal modes in terms of CN and CX (X = H or F) are quite different for the two molecules and therefore inferences made about the bonding from the vibrational spectra are best based on force constants. Another example is provided by the vibrational spectrum of ethylene adsorbed on metal surfaces, which is often described as bonding in either a di-σ or π form [6]. The distinction rests largely on whether or not the CC bond order is 1 or 2. Yet extracting the bond order from the vibrational spectrum is problematical because the CC stretch, CH_2 bend, and CCH_2 wag internal coordinates all make significant contributions to the normal modes with fundamentals in the region of 900 to 1600 cm^{-1}. Stuve and Madix [7] proposed a method of parameterizing spectra of adsorbed ethylene in order to classify the bonding as di-σ or π. While this particular parameterization may be useful for ethylene, a normal mode analysis is of far greater generality. Specifically, if normal coordinate analyses were available for various forms of adsorbed ethylene, then the optimized CC force constant would readily yield the desired information. In addition to obtaining force constants based on internal coordinates, the composition of the normal modes is also obtained from the analysis. Among other advantages, this removes the ambiguity in naming the observed bands. The common practice is to name an observed fundamental according to the internal coordinate that makes the biggest contribution to the normal mode being excited. For adsorbed ethylene, a strong reduction in CC bond order upon adsorption occurs and the fundamental of the mode with more CC stretch than CH_2 bend character can have a lower frequency than the fundamental with more CH_2 bend character, making the relative frequencies opposite that of the gas phase molecule [8]. This point has resulted in considerable confusion in the literature. Furthermore, a lack of appreciation of the extent to which the normal modes are composed of two or more internal coordinates leads to confusion as to whether observed isotopic shifts are reasonable. The routine use of normal coordinate analyses of surface vibrational spectra can largely eliminate the type of confusion and ambiguity that has been associated with the surface vibrational literature of ethylene, and other molecules.

In addition to obtaining force fields from a normal mode analysis of experimental frequencies, force fields can also be obtained through ab initio electronic structure calculations. Fogarasi and Pulay [9,10] have considered in detail the issue of ab initio force fields and discuss their relationship to experimental force fields. They note that even for small gas phase molecules, the dominant force constants are still more accurately determined experimentally. However, ab initio methods can provide better values for the weaker interaction force constants. Electronic structure calculations of molecules adsorbed on surfaces is a well-developed subject [11–15] that is evolving rapidly. Vibrational frequencies are often reported from such calculations rather than force fields. Yet as Fogarasi and Pulay have noted [9,10], the calculation of force fields based on internal coordinates offers considerable advantages over a calculation of frequencies alone. The increasing

availability of experimental force fields determined through normal mode analyses of surface vibrational data as described here, and by others [16–18], should serve to stimulate the calculation of the corresponding ab initio force fields.

The normal coordinate analyses used in the characterization of four distinct adsorbates, namely CNH_2, CNH_2 dimers, HCNH, and $(CNH_2)_2$ are reviewed here. The simplest species, aminomethylidyne (CNH_2), has been observed on Pt(111) during the thermal decomposition of both hydrogen cyanide (HCN) and methylamine (CH_3NH_2) [19–21], while CNH_2 aggregates are generated through the decomposition of azomethane ($CH_3N_2CH_3$) as well as high coverages of HCN [19,21,22]. We have also recently shown that a diiminium species, diaminoethylene ($H_2NC{=}CNH_2$), is formed via the hydrogenation of cyanogen (C_2N_2) on Pt(111) [21,23–25]. In each of these studies [19–25], normal mode calculations not only proved instrumental in identifying the adsorbates formed, but also provided unique insights into the nature of their internal bonding.

2. Experimental

The Fourier transform reflection absorption infrared spectroscopy (FT-RAIRS) experiments were carried out in a stainless steel ultra high vacuum (UHV) chamber with a base pressure of $\sim 1 \times 10^{-10}$ Torr. A detailed description of this system can be found elsewhere [26]. All spectra were recorded at either 85 or 300 K, using 1024 or 2048 co-added scans with a resolution of 4 cm^{-1}. Two types of infrared detector were used. An MCT detector was used to obtain spectra between 4000 and 800 cm^{-1}, while an InSb detector with a low wavenumber cut off of 1900 cm^{-1} was used to obtain complementary spectra above 1950 cm^{-1}. The preparation and purification of HCN and C_2N_2, as well as their ^{13}C and ^{15}N isotopically substituted analogues, is discussed in detail elsewhere [20,23,27]. The crystal surface was in each case exposed to the appropriate gas or gases by back filling the chamber via a leak valve. The exposures of all gasses used were derived from uncorrected ion gauge readings, where 1 Langmuir (L) $= 1 \times 10^{-6}$ Torr s.

3. Normal mode calculations

The Wilson FG matrix method [3] has long been used for normal mode calculations. Its popularity stems in part from the use of familiar stretch, bend, wag, and torsion internal coordinates as basis functions. The force constants defined in terms of internal coordinates are readily associated with the notion that molecules are held together by bonds connecting adjacent atoms. Alternatively, normal modes can be expressed in terms of the Cartesian coordinates of each atom, a choice that offers some mathematical conveniences but does not yield a set of force constants that can be readily interpreted in terms of the relative ‘stiffnesses’ of chemical bonds. The practical implementation of the FG matrix method is conveniently achieved with a set of computer programs written by McIntosh and Peterson [28]. A full description of how this set of programs was used in the normal mode analyses described here is presented elsewhere [29]. For the most part, the use of these programs for adsorbates on surfaces is similar to their general use. Thus, the basic input is a molecular geometry and a set of initial force constants. Unfortunately, accurate values for bond lengths and angles for adsorbates are available for only a few special cases, while accurate structural information is generally available for the non-surface cases. Fortunately, the results are not very sensitive to small variations of geometric parameters. In the cases described below, we chose geometric parameters and force constants typical of compounds with similar functionalities to the proposed adsorbates. Although the Cartesian coordinates and masses of the atoms are in principle sufficient information to define the **G** matrix, the set of

internal coordinates to be used must also be specified since this is not uniquely defined from atomic positions alone. The symmetry of the molecule is used in the analysis only if explicitly entered.

While the focus of this paper is on the $3N-6$ internal modes of the adsorbates, the fact that the adsorbate is attached to a surface is taken into account by including a few platinum atoms. This permits us to calculate frequencies for the three frustrated translations and three frustrated rotations, the degrees of freedom that would be pure rotations and translations of the free molecule. There are obviously some aspects of the actual system that cannot be described by such a simplified treatment. For example, the low frequency modes involving substrate atom motion and the dispersion associated with two-dimensional adsorbate phonon bands cannot be dealt with. However, since we are only measuring vibrations above about 800 cm^{-1} and because adsorbate–adsorbate interactions are weak relative to the internal bonding of the adsorbates considered here, the models are appropriate for the data. Furthermore, the data is typical of that

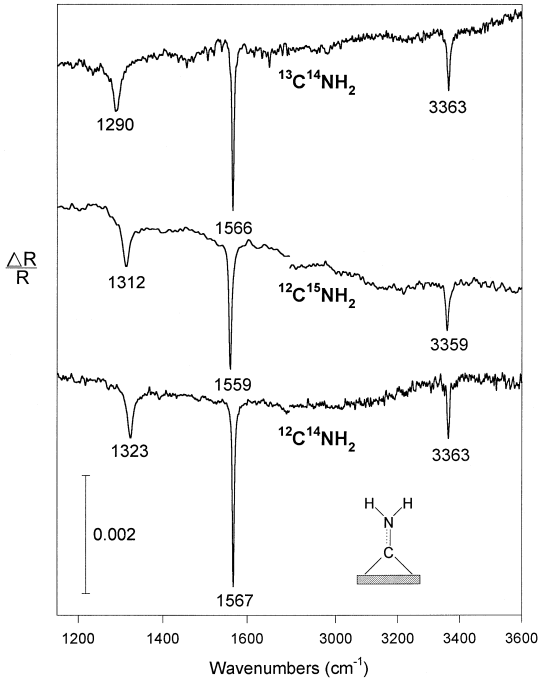

Fig. 1. Spectra of isotopically substituted aminomethylidyne (CNH_2), derived from $H^{13}C^{14}N$, $H^{12}C^{15}N$ and $H^{12}C^{14}N$ at 300 K. All spectra were acquired with an MCT detector.

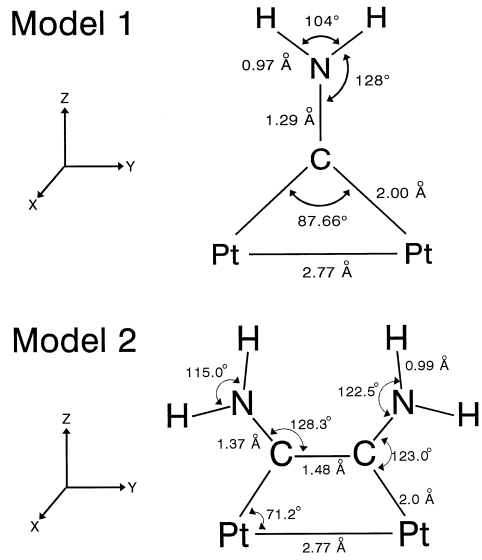

Fig. 2. Spectra of isotopically substituted diaminoethylene ($(CNH_2)_2$), derived from the hydrogenation of $^{12}C_2^{14}N_2$, $^{12}C_2^{15}N_2$ and $^{13}C_2^{14}N_2$ at 300 K. Spectra were acquired using an MCT detector between 800 and 1900 cm^{-1} and with an InSb detector from 1900–4000 cm^{-1}.

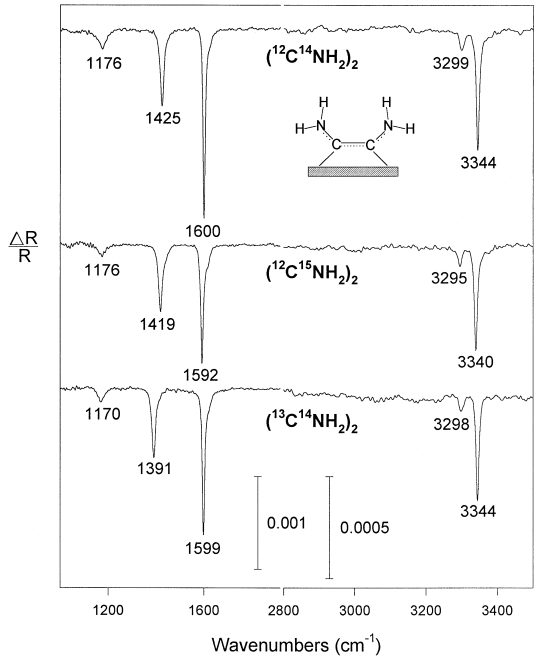

Fig. 3. Geometric models representing likely structures CNH_2 (model 1) and $(CNH_2)_2$ (model 2) adopt on Pt(111).

obtained in most RAIRS studies and the methods used here should have wide applicability.

For the spectra of Fig. 1, HCNHPt and $(CNH_2)Pt_2$ models, corresponding to different interpretations of essentially identical spectra [20,30], were used. A schematic diagram of the $(CNH_2)Pt_2$ model is shown in Fig. 3 (model 1). Two $C_{2\nu}$ symmetry $(CNH_2)_2Pt_2$ models, based on the perpendicular and parallel μ_2, η^2-bonding modes acetylinic and di-metalated olefinic ligands adopt in organometallic clusters [31,32], were constructed to model the spectra of Fig. 2. A schematic diagram of the olefinic or 'parallel' $(CNH_2)_2Pt_2$ model is shown in Fig. 3 (model 2). Spectra observed during both aminomethylidyne aggregation and diaminoethylene decomposition (Fig. 4) were modeled using a $(CNH_2)(CNH_2)Pt_3$ aminomethylidyne dimer model (Fig. 5). A complete listing of all of the geometric parameters for each model used in the calculations can be found within the corresponding publications [22,24]. In each case, the platinum atoms were assigned effectively infinite masses while the force constant joining them was made essentially rigid by assigning it an arbitrarily large value of 50 mdyn $Å^{-1}$. For the linear Pt_3 chain of the aminomethylidyne dimer model, the bending force constant was assigned an arbitrarily large value of 30 mdyn Å rad^{-2}. The primary force constants corresponding to the internal coordinates of the adsorbates were taken from analogous compounds. For example, the initial HNC bend force constant used for $(CNH_2)Pt_2$ was taken from an ab initio study of $HNCH_2$ [33].

In addition to the primary force constants associated with each internal coordinate a number of interaction (off-diagonal) force constants

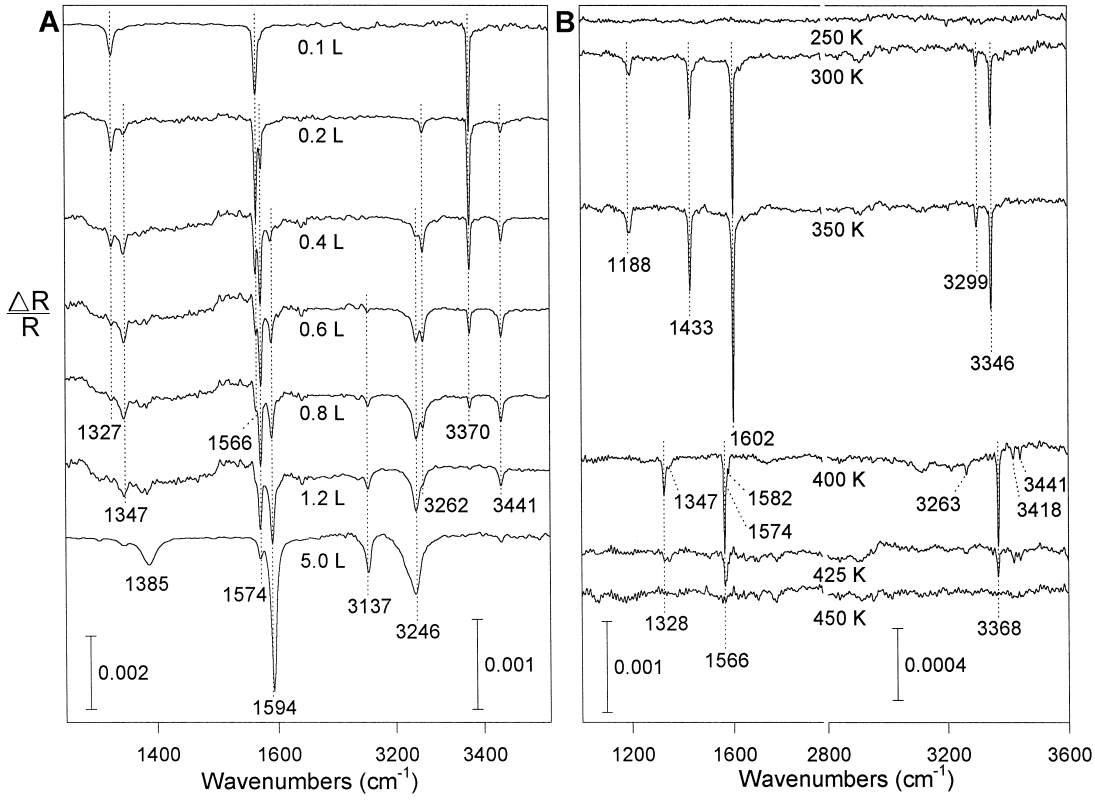

Fig. 4. Spectra acquired during studies of CNH_2 aggregation (A) and $(CNH_2)_2$ thermal decomposition (B). The spectra in each study were acquired using an MCT detector between 800 and 1900 cm^{-1} and with an InSb detector from 1900–4000 cm^{-1}.

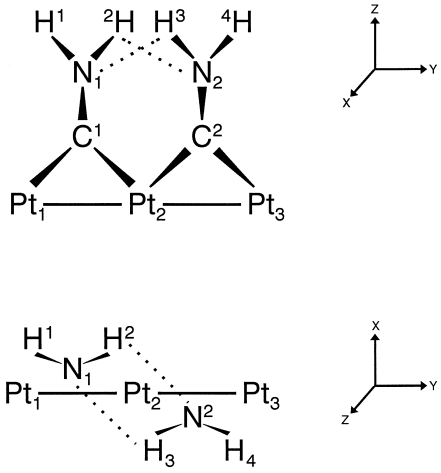

Fig. 5. Geometric models representing likely structure an aminomethylidyne dimer may adopt on Pt(111). Each CNH_2 moiety forms a pair of cooperative N–H$\cdot\cdot\pi$ hydrogen bonds. The carbon atoms of each CNH_2 unit have been omitted for clarity in the lower figure.

were also included. Although the number of interaction constants can in principle be prohibitively large, leading to far more fitting parameters than independent frequencies, several factors limited the number actually needed. Since the models used in each case were highly symmetric they contained a number of degenerate internal coordinates possessing identical primary force constants. Also, many are negligibly small or are identically equal to zero by symmetry. Only coupling constants between internal coordinates that have the same symmetry, that also have primary force constants of similar magnitude, and that share one or more common atoms, were considered.

A fortuitous aspect of the adsorbates considered here is that an extensive number of isotopomers could be generated from ^{12}C, ^{13}C, ^{14}N, ^{15}N, ^{1}H, and ^{2}H. The relatively large number of discrete experimental frequencies allowed the number of unique force constants of each model to be set to less than or equal to the number of observable bands, which had the effect of producing a reliable set of 'best fit' force constants from the optimization procedure. Once a best fit set of force constants had been determined, the composition of the normal modes, their corresponding frequencies, and the relative isotopic shifts for each model were reevaluated. A model was deemed successful when, in conjunction with accurately modeled relative isotopic shifts, the RMS error between calculated and observed frequencies was $\sim$20–40 cm^{-1}, while the force constants deviated by no more than 5–10% from their initial values. Due to the fact that the FG matrix method relies upon an harmonic approximation of a coordinate's potential energy, it is unrealistic to expect RMS values better than $\sim$20–30 cm^{-1}, since anharmonic contributions to the potential are generally of this order. Although the RMS error in frequency for several unsuccessful models was also found to optimize to around 20–30

Table 1
Initial and optimized force constant parameters for $(CNH_2)Pt_2$. Units of force constants are mdyn $Å^{-1}$ for bond stretches and mdyn Å rad^{-2} for bends, wags and torsions

Internal coordinate	Initial force constant (mdyn $Å^{-1}$)	Final force constant (mdyn $Å^{-1}$)	Δ force constant (%)	Source
N–H bond stretch	6.383	6.361	−0.34	CH_3NH_2 [a]
N–C bond stretch	6.540	6.198	−5.23	$NNCH_2$
C–Pt bond stretch	2.450	2.611	+6.57	CH_3C–Pt
Pt–Pt bond stretch	50.00	49.99	−0.02	Assigned
H–N–H bend	0.173	0.169	−2.31	CF_3CONH_2
H–N–C bend	0.882	0.870	−1.36	$HNCH_2$
N–C–Pt bend	1.500	1.533	+2.20	CH_3C–Pt
C–N–H–H wag	0.643	0.658	+2.33	$CH_3CH_2NH_2$
N–C–Pt–Pt wag	0.260	0.228	−12.31	C_2H_4
C–N bond torsion	0.050	0.048	−4.00	$CH_3CH_2NH_2$

[a] Details pertaining to all geometric and force constant parameters can be found in Ref. [22].

Table 2
Force constant parameters for $(CNH_2)_2Pt_2$ and $(CND_2)_2Pt_2$. Units of force constants are mdyn Å^{-1} for bond stretches and mdyn Å rad^{-2} for bends, wags and torsions

Internal coordinate	Initial force constant	$Pt_2(C_2N_2H_4)$ force constant	$Pt_2(C_2N_2D_4)$ force constant	Source
N–X stretch	6.361	6.055	5.937	CNH_2[a]
C–N stretch	6.198	8.274	7.970	CNH_2
C–Pt stretch	2.611	2.135	2.152	CNH_2
C–C stretch	7.600	8.377	8.060	C_6H_6
Pt–Pt stretch	50.00	50.63	50.57	Assigned
X–N–X bend	0.169	0.126	0.311	CNH_2
X–N–C bend	0.870	0.975	1.122	CNH_2
N–C–C bend	0.700	0.628	0.592	pyrrole
N–C–Pt bend	1.533	2.907	3.020	CNH_2
C–N–X–X wag	0.658	0.627	0.651	CNH_2
N–C–Pt–Pt wag	0.288	0.288	0.200	CNH_2
C–N torsion	0.048	0.038	0.036	CNH_2
C–C torsion	0.197	0.225	0.251	retinal
NX–NX st–st	0.198	0.270	0.265	CNH_2
NX–CN st–st	0.087	0.074	0.164	CNH_2
CC–CN st–st	0.250	0.487	0.539	pyrrole

X = H or D.
[a] Details pertaining to all geometric and force constant parameters can be found in Ref. [24].

Table 3
(a) Initial perturbation of $(CNH_2)Pt_2$ monomer force constants necessary to model analogous H-bond internal coordinates of the $(CNH_2)(CNH_2)Pt_3$ dimer model

Internal coordinate	Optimized monomer f.c. (mdyn Å^{-1})	Initial dimer f.c. (mdyn Å^{-1})	Δ (%)
ν(NH)[a]	6.361	5.916	−7.00
ν(CN)[a]	6.198	6.736	+8.69
δ(HNC)[a]	0.870	0.926	+6.44

(b) Initial and final optimized force constants for the $(CNH_2)(CNH_2)Pt_3$ aminomethylidyne dimer model

Internal coordinate	Initial dimer f.c. (mdyn Å^{-1})	Optimized dimer f.c. (mdyn Å^{-1})	Δ (%)
ν(NH)	6.361	6.270	−1.43
ν(NH)[a]	5.916	5.817	−1.67
ν(NH)ν(CN)	0.087	0.087	0.00
ν(CN)[a]	6.736	6.833	+1.44
ν(CPt)	2.611	2.752	+5.40
ν(PtPt)	49.99	50.11	+0.24
δ(HNC)	0.870	0.868	−0.23
δ(HNC)[a]	0.926	0.910	−1.73
δ(NCPt)	1.533	1.526	−0.46
$\rho(CNH_2)$	0.658	0.651	−1.06
$\rho(NCPt_2)$	0.228	0.229	+0.44
$\tau(H_2NCPt_2)$	0.048	0.049	+2.08
δ(PtPtPt)	30.00	30.02	+0.07
ν(NH)[b]	0.300	0.304	+1.33
δ(NHN)[b]	0.026	0.025	−3.85

[a] Denotes coordinates defining the H-bond *within* CNH_2 units.
[b] Denotes 'new' coordinates defining the H-bond *between* CNH_2 units.

cm^{-1}, these models were deemed to be erroneous since the best fit force constants were in some cases altered by a factor of 2 or more from their closely related initial values, while the relative isotopic shifts were also poorly modeled. A complete listing of all initial and optimized force constants for each successful model can be found in Table 1 (CNH_2); Table 2 ($(CNH_2)_2$); Table 3a and b (CNH_2 dimer), as well as within the corresponding publications [22,24].

4. Results and discussion

4.1. The characterization of aminomethylidyne, CNH_2

The RAIR spectra of Fig. 1 were recorded at 300 K following separate 0.2 L exposures of $H^{12}C^{14}N$, $H^{13}C^{14}N$, and $H^{12}C^{15}N$ on Pt(111). The positions and isotopic shifts observed for the bands of the species derived from HCN, given in Table 4a and b, are discussed in detail elsewhere [20]. Essentially identical spectra, assigned to CNH_2 derived from $H^{12}C^{14}N$, have also been recorded during RAIRS studies of CH_3NH_2 thermal decomposition [19,30] and CN hydrogenation [21,23,25] on Pt(111), while similar HREEL spectra have also been observed during the decomposition of CH_3NH_2 on Pt(111) [30] and HCN on Pd(111) [34]. Even though the spectra observed in each case are very similar, they have been attributed to one of three distinct adsorbates. Kordesch et al. [34] assigned HREEL bands at 3307–3347 cm^{-1}, 1540 cm^{-1} and 1331 cm^{-1}, respectively, to the ν(CH), ν(CN) and δ(HCN) modes of a rehybridized HC=N species formed from HCN on Pd(111) at 300 K. This model is not consistent with the RAIRS spectra from HCN on Pt(111)

Table 4

(a) Experimental and calculated frequencies (cm^{-1}) for aminomethylidyne, CNH_2

Isotopomer		ν_a(NX)	ν_s(NX)	δ(NXX)	ν(CN)
$^{12}C^{14}NH_2$	Expt.	–	3363	1567	1323
	Calc.	3456	3360	1570	1298
$^{13}C^{14}NH_2$	Expt.	–	3363	1566	1290
	Calc.	3456	3360	1564	1267
$^{12}C^{15}NH_2$	Expt.	–	3359	1559	1312
	Calc.	3445	3353	1559	1292
$^{12}C^{14}ND_2$	Expt.	–	2435	1356	
	Calc.	2559	2452	1390	1054
$^{12}C^{15}ND_2$	Expt	–	2425	1340	–
	Calc	2544	2441	1376	1053
$^{12}C^{14}NHD$	Expt.	3430	2527	1439	–
	Calc.	3408	2507	1526	1387
$^{12}C^{15}NHD$	Expt.	3421	2521	1426	–
	Calc.	3400	2494	1508	1344

(b) Experimental and calculated relative isotopic shifts (cm^{-1}) of aminomethylidyne, CNH_2

Mode		($^{12}C^{15}NH_2$) ($^{12}C^{14}NH_2$)	($^{13}C^{14}NH_2$) ($^{12}C^{14}NH_2$)	($^{12}C^{14}ND_2$) ($^{12}C^{14}NH_2$)	($^{12}C^{15}ND_2$) ($^{12}C^{14}ND_2$)	($^{12}C^{15}NHD$) ($^{12}C^{14}NHD$)
$\nu(NX)_s$	Expt.	−4	0	−928	−10	−9(H) −6(D)
$\nu(NX)_s$	Calc.	−7	0	−908	−11	−8(H) −13(D)
$\delta(NX_2)$	Expt.	−8	−1	−211	−16	−13
$\delta(NX_2)$	Calc.	−11	−6	−180	−14	−18
ν(CN)	Expt.	−11	−33	–	–	–
ν(CN)	Calc.	−6	−31	−244	−1	−43

X = H or D.

at 300 K since the absolute frequency and isotopic shifts of the 3363 cm^{-1} band indicate that it is due to an NH rather than CH stretch. Erley and Hemminger [30] assigned HREEL and RAIR bands at 3371 cm^{-1}, 1565 cm^{-1} and 1325 cm^{-1}, obtained from the thermal decomposition of CH_3NH_2 on Pt(111), to the ν(NH), ν(CN) and δ(HCN) modes of an HCNH species [35] in which the CH stretch was oriented such that it was too weak to detect with RAIRS. In an effort to distinguish between HCNH and CNH_2 on the basis of our observed spectra, we carried out normal mode analyses using structural models of both adsorbates.

The $(CNH_2)Pt_2$ model was constructed using the geometric and force constant parameters shown in Fig. 3 (model 1) and Table 1. The geometric parameters used were largely based on similar coordinates found in both $Os_3(\mu\text{-}CNH_2)(CO)_{10}$ [36] and $Ru_3(\mu\text{-}CN(CH_3)_2(CO)_{10}$ [37,38] clusters, as well as a number of other complementary sources [22]. A total of 14 primary force constants, 10 of which were unique, and two interaction force constants were used throughout the calculations. Based on analogous species [22], initial values of 0.0197 and 0.087 mdyn $Å^{-1}$ respectively were assigned to the two NH–NH and NH–CN interaction force constants. Of the 12 possible isotopomers of aminomethylidyne that can be produced through substitution with ^{13}C, ^{15}N and D, seven were generated. This in turn allowed for a total of 21 experimental bands to be observed, as displayed in Table 4a. Of these 21 bands, 13 were recorded for five high symmetry $^{12}C^{14}NH_2$, $^{13}C^{14}NH_2$, $^{12}C^{15}NH_2$, $^{12}C^{14}ND_2$, and $^{12}C^{15}ND_2$ isotopomers, while the remainder were the lower symmetry $^{12}C^{14}NHD$ and $^{12}C^{15}NHD$ 'mixed' species. Since the number of observed bands recorded for the fully hydrogenated or deuterated species exceeded the number of unique force constants used throughout the corresponding calculations, the criteria necessary for an accurate optimization of the components of the **F** matrix was satisfied. The optimized force constants derived for the five $C_{2\nu}$ symmetry models are displayed in Table 1. It can be seen that the initial force constants were only perturbed on average by $\pm 3.7\%$ upon optimization. Having established a reliable set of optimized force constants for the fully hydrogenated and deuterated species, these values were subsequently used to calculate frequencies for two C_s symmetry $(^{12}C^{14}NHD)Pt_2$ and $(^{12}C^{15}NHD)Pt_2$ models. As Table 4a demonstrates, the frequencies derived for all seven models are in close agreement with the experimental values, with the $C_{2\nu}$ symmetry species having an overall RMS error of 22 cm^{-1}. The relative isotopic shifts of each species were also accurately modeled (Table 4b).

The HCNHPt model was constructed using geometric parameters consistent with the structure of an $HFe_3(CH_3C{=}NH)(CO)_9$ cluster [39], as well as the proposed orientation and bonding of HCNH on Pt(111) [30], which is somewhat similar to what was proposed for HCNH on W(100)–(5×1)–C [35]. Since the only symmetry element in the proposed structure of HCNH is the molecular plane, isotopic substitution cannot reduce the symmetry and all HCNH isotopomers belong to the C_s point group. The initial force constant values were taken from a variety of sources, including H_2CNH [33] and $Pt(CH_3CN)_2$ [40]. A total of 11 force constants, 9 primary and 2 interaction, were used. A complete listing of all geometric parameters and initial force constants are given elsewhere [29]. As for CNH_2, the number of observed bands (14) exceeded the number of force constants. The bands derived from $H^{12}C^{14}N$ at 3363, 1567 and 1323 cm^{-1}, were assigned to the respective ν(NH), ν(CN) and δ(HCN) modes of the HCNHPt model. The force constants of the HCNHPt model were found to vary greatly upon optimization, by an average of $\pm 24.51\%$ from their initial values, while the best fit frequencies were found to have an RMS error of 108 cm^{-1}.

A comparison of the results obtained from the $(CNH_2)Pt_2$ and HCNHPt calculations clearly demonstrate that the $(CNH_2)Pt_2$ model is in better agreement with the experimental

spectra. The RMS error between calculated and observed frequencies for $(CNH_2)Pt_2$ was found to be much better than for HCNHPt (22 versus 108 cm^{-1}), while the differences between initial and optimized force constants followed a similar trend (± 3.7 versus $\pm 24.5\%$). A comparison of the calculated and experimental isotope shifts for the two models shows clear differences, particularly for the modes with fundamentals in the mid-IR region. These modes contain significant contributions from a number of internal coordinates. For example, the $\delta(NH_2)$ mode of the $(CNH_2)Pt_2$ model was found to be composed of significant contributions from both HNH bend (56%) and CN stretch (20%) internal coordinates. Thus, a comparison of each model's calculated relative isotopic shifts with those observed experimentally, for modes giving rise to fundamentals at 1567 and 1323 cm^{-1}, should necessarily provide insight into the validity of each model, since these bands were assigned to the $\delta(NH_2)$ and $\nu(CN)$ modes of $(CNH_2)Pt_2$ while for HCNHPt they were assigned to dissimilar $\nu(CN)$ and $\delta(HCN)$ modes. As demonstrated by Table 4b, the relative isotope shifts observed experimentally are close to those calculated for the $(CNH_2)Pt_2$ model. For example, a shift of -33 cm^{-1} is observed for the 1323 cm^{-1} band under ^{13}C substitution, while a shift of -31 cm^{-1} is calculated for the $\nu(CN)$ mode of $(CNH_2)Pt_2$. This is not true for the analogous band assigned to the $\delta(HCN)$ mode of HCNHPt, which is calculated to shift by only -2 cm^{-1}. Of particular interest are differences in relative isotope shifts calculated for the 1567 cm^{-1} band under complete ^2H substitution, a shift of -211 cm^{-1} is observed experimentally, while shifts of -180 and $+124$ cm^{-1} are calculated for the respective $\delta(ND_2)$ and $\nu(CN)$ modes of $(CND_2)Pt_2$and DCNDPt. The better agreement for the isotopic shifts, the lower RMS error between experimental and calculated frequencies, as well as the smaller change of the optimized force constants from their initial values favor the assignment of the spectra of Fig. 1 to CNH_2, rather than to HCNH.

An independent ab initio study of the chemisorption of CNH_2 and HCNH on Ni(111) [13] endorses the findings discussed above. It was shown [13] that CNH_2 is planar; bonds to the substrate through carbon at a bridge site; and possesses $\nu(NH)$ and $\nu(CN)$ modes which give rise to frequencies at 3356 and 1335 cm^{-1}. The HCNH adsorbate, in contrast, is shown to bond to the surface at an adsorption site intermediate between a bridge and 3-fold hollow, with the CN axis parallel to the surface; and to have $\nu(NH)$, $\nu(CH)$ and $\nu(CN)$ at 3349, 2935 and 1457 cm^{-1}, respectively. Both CNH_2 and HCNH were found to be stable on Ni(111), with respective adsorption energies of 56.6 and 88.2 kcal mol^{-1}. Significantly, the authors point out that the vibrational frequencies derived for both CNH_2 and HCNH on Ni(111) are consistent with the experimental evidence that CNH_2 and HCNH are formed on Pt(111) [30] and W(100)–(5×1)–C [35] respectively. While the HCNH adsorbate is evidently more stable than CNH_2 by some 31.7 kcal mol^{-1}, it is assumed that the energetics of formation of these two stable, yet distinctly different, adsorbates on Pt(111) and W(100)–(5×1)–C determine which of these species is ultimately generated. While the results of this electronic structure calculation [13] confirm that a planar bridge bound CNH_2 species is most likely formed on Pt(111), a more detailed comparison of the results of this study with those of the normal mode analysis presented above reveal numerous additional similarities. Firstly, the geometric parameters derived for CNH_2 on Ni(111) are highly similar to those taken from literature sources, and subsequently used throughout the normal coordinate analyses. Bond lengths of 1.02, 1.32 and 2.02 Å; as well as an HNH bond angle of $115\pm5°$; were calculated for the corresponding N–H, C–N, C–Ni and HNH coordinates of CNH_2 on Ni(111), while values of 0.97 Å, 1.29 Å, 2.00 Å and 104° were used for the analogous coordinates of $(CNH_2)Pt_2$. The similarities between these two sets of geometric parameters validate the choice of values used in the normal

coordinate calculation. However, in order to test the effect of small changes among crucial bond lengths and angles of the $(CNH_2)Pt_2$ model, a sensitivity analysis, in which the r(CN) and $\angle$HNH coordinates were altered by up to ± 0.5 Å and $\pm 15°$, was performed [22,29]. It was shown that the frequencies calculated with these changes, which encompass the values of equivalent geometric parameters derived from the analogous ab initio study, were insensitive to such alterations. Secondly, the frequencies derived for the ν(NH) and ν(CN) modes of CNH_2 are in both cases very similar to the 3363 and 1323 cm^{-1} values observed experimentally, as frequencies of 3360 and 1298 cm^{-1} were obtained from the normal coordinate analysis; while values of 3356 and 1335 cm^{-1} were derived from the electronic structure calculation. Unfortunately, because only frequencies were reported in the ab initio study, we cannot make a direct comparison between our experimental force field and an ab initio force field for CNH_2. Also, only vibrational frequencies for the stretch coordinates were derived [13], precluding a comparison of the vibrational frequencies associated with bend, wag and torsional motions.

4.2. The characterization of diaminoethylene, $(CNH_2)_2$

The interpretation of the FT-RAIRS spectra shown in Fig. 2, due to three hydrogenated cyanogen isotopomers, has been described in detail elsewhere [23,24]. Briefly, the band positions and relative isotopic shifts, displayed in Table 5a and b, show that the 3344, 3299, 1600, 1425 and 1176 cm^{-1} bands are due to the respective $\nu(NH)_{sym}$, $\nu(NH)_{sym}$, $\delta(NH_2)$, ν(CN) and ν(CC) modes of a di-iminium sur-

Table 5

(a) Experimental and calculated frequencies (cm^{-1}) of diaminoethylene, $(CNH_2)_2$

Isotopomer		$\nu(NX)_s$)	$\nu(NX)_s$	$\delta(NX_2)$	ν(CN)	ν(CC)
$(^{12}C^{14}NH_2)_2$	Expt.	3344	3299	1600	1425	1176
	Calc.	3349	3300	1612	1439	1152
$(^{12}C^{15}NH_2)_2$	Expt.	3340	3295	1592	1419	1176
	Calc.	3343	3289	1599	1435	1144
$(^{13}C^{14}NH_2)_2$	Expt.	3344	3298	1599	1391	1170
	Calc.	3349	3300	1604	1427	1133
$(^{12}C^{14}ND_2)_2$	Expt.	2442	2409	1460	1280	–
	Calc.	2443	2407	1485	1236	993
$(^{12}C^{15}ND_2)_2$	Expt.	2436	2405	1446	1274	–
	Calc.	2426	2398	1469	1233	987
$(^{13}C^{14}ND_2)_2$	Expt.	2440	–	1430	1254	–
	Calc.	2442	2407	1471	1224	983

(b) Experimental and calculated relative isotopic shifts (cm^{-1}) of diaminoethylene, $(CNH_2)_2$

Mode		$(^{12}C^{15}NH_2)_2$ / $(^{12}C^{14}NH_2)_2$	$(^{13}C^{14}NH_2)_2$ / $(^{12}C^{14}NH_2)_2$	$(^{12}C^{14}ND_2)_2$ / $(^{12}C^{14}NH_2)_2$	$(^{12}C^{15}NH_2)_2$ / $(^{12}C^{14}NH_2)_2$
$\nu(NX)_g$	Expt.	−4 (−4)[a]	0 (0)	−902 (928)	−6 (−10)
$\nu(NX)_g$	Calc.	−6	0	−906	−17
$\nu(NX)_g$	Expt.	−4	−1	−890	−4
$\nu(NX)_g$	Calc.	−1	0	−893	−9
$\delta(NX_2)$	Expt.	−8 (−8)	1 (−1)	−140 (−211)	−14 (−16)
$\delta(NX_2)$	Calc.	−13	−8	−127	−16
ν(CN)	Expt.	−6 (−11)	−34 (−33)	−145	−6
ν(CN)	Calc.	−4	−12	−203	−3

[a] Values in parentheses are for aminomethylidyne (CNH_2).
X = H or D.

face species of general formula $(CNH_2)_2$. The band positions, intensities and relative isotopic shifts of $(CNH_2)_2$ are almost identical to the analogous bands of aminomethylidyne (CNH_2) [20], as shown in Table 5b. This suggests that both species possess similar internal coordinates and iminium-$(C{=}NH_2)$ like functionalities. The low number of observed bands in the spectra imply that the $(CNH_2)_2$ adsorbate is planar, has a high degree of symmetry, and most likely bonds to the substrate through both carbon atoms with a μ_2,η^2- or bridge configuration. As for aminomethylidyne, the number and frequencies of the additional NH and ND stretch bands observed for partially deuterated isotopomers is indicative of reducing the symmetry from $C_{2\nu}$ to C_s. A detailed description of the bands arising from the partial deuteration of $(CNH_2)_2$ can be found elsewhere [29].

Numerous surface and organometallic studies [31,32,41–43] of analogous adsorbates and ligands indicate that the $(CNH_2)_2$ plane may adopt one of three possible bonding configurations with respect to the Pt surface: it may be tilted with respect to the surface normal, or it may be perpendicular to the surface but either parallel or perpendicular to the line between the two Pt atoms to which it is bonded. We refer to these three configurations as tilted, parallel, or perpendicular. The parallel configuration is often associated with olefinic bonding, and the perpendicular one with acetylinic bonding. Acetylinic (C_2H_2) adsorbates have been shown by LEED to adopt asymmetric C_s symmetry geometries at 3-fold adsorption sites on Pt(111) [41] and Pd(111) [42]. In conjunction with angle-dependent EELS measurements [43], it is surmised that these types of highly perturbed acetylinic adsorbates possess carbon atoms of $\sim sp^{2.5}$ hybridization and are tilted by ~ 19 degrees from the surface normal. Upon tilting a planar $(CNH_2)_2$ species, the plane of symmetry perpendicular to the C–C axis is retained but the molecular plane is no longer a symmetry element and formerly forbidden vibrations that were perpendicular to the molecular plane in the $C_{2\nu}$ configuration become allowed. A tilted adsorption geometry for $(CNH_2)_2$ was rejected since the low number of observed bands is not consistent with the higher number of allowed A′ modes expected of a C_s symmetry $(CNH_2)_2$ species. To gain further insight into the nature of the adsorbate a series of normal mode calculations, using parallel and perpendicular $(CNH_2)_2Pt_2$ models were performed and are discussed in detail below.

The geometric parameters used in the construction of the two $(CNH_2)_2Pt_2$ models are discussed in detail elsewhere [24], while parameters used for the parallel olefinic model are also shown in Fig. 2 (model 2). A total of 16 unique initial force constants (13 diagonal and 3 off-diagonal), taken from the closely related compounds shown in Table 2, were used in each calculation. We used three off-diagonal NH–NH, NH–CN and CN–CC stretch–stretch interaction force constants, for reasons discussed in Section 3. Calculations using the initial force constants showed that both models produced reasonably good fits to the data. The RMS errors recorded for differences between calculated and observed frequencies were 84 and 104 wavenumbers respectively for the parallel olefinic and perpendicular acetylinic models. The ν(CC) mode of the perpendicular model was poorly modeled however, even when a force constant characteristic of a CC single bond was substituted for the initial value of 7.6 mdyn $Å^{-1}$. In contrast to the similar RMS fits observed for both models using the initial force constants, frequencies generated using optimized force constants show that the parallel $(CNH_2)_2Pt_2$ model yields better agreement with the observed spectra. Frequencies calculated for the parallel model achieved an RMS error of 18 cm^{-1}, while the RMS error of the perpendicular model remained practically identical to the 104 cm^{-1} value obtained using the original constants. In an analogous calculation using a parallel $(CND_2)_2Pt_2$ model and identical initial force constants to those used with the $(CNH_2)_2Pt_2$ calculation, an RMS error of 26 cm^{-1} was

obtained for the fully deuterated isotopomers. The force constants derived from each optimization procedure were again deemed to be reliable best fit solutions, since a total of 27 discrete experimental frequencies, shown in Table 2, were utilized by the fitting program. Although these models are simplified interpretations of only two possible types of bridge adsorption site, these results do show that the parallel geometric model, which contains an approximate C=C double bond and two C–Pt bonds, is more representative of the adsorbate that gives rise to the observed spectra than the corresponding perpendicular model, which possesses a near C–C single bond and four C–Pt bonds. Thus, the results of these normal mode calculations, in terms of the calculated absolute frequencies, relative isotopic shifts and the best fit force constants of both $(CNH_2)_2Pt_2$ models are strongly supportive of the hypothesis that μ_2,η^2-diaminoethylene ($H_2NC{=}CNH_2$), bonding to the surface with a parallel di-metalated olefin configuration, is formed by the reaction of cyanogen and hydrogen on Pt(111). If the initial and optimized force constants displayed in Table 2 are examined it can be seen that the values for the CN stretch, CC stretch and NCPt bend internal coordinates for $(CNH_2)_2Pt_2$ increase upon optimization, while the remainder of the primary force constants remain relatively unaltered from their initial values. The 8.274 mdyn $Å^{-1}$ value of the CC force constant implies a bond order of $\sim$1.8, which is consistent with the adsorbate bonding in a di-metalated olefinic mode, and is similar to the value of the C=C bond in ethylene (9.15 mdyn $Å^{-1}$) [44]. The CN bond must still be classified as an 'iminium like' partial double bond since the calculated value of 3.377 mdyn $Å^{-1}$, although slightly higher than the aminomethylidyne (CNH_2) value, is still substantially lower than that of a C=N double bond (11.84 mdyn $Å^{-1}$) [44]. The increase in the NCPt bend force constant is most likely a consequence of the increase in the CC and CN stretch force constants. A closer examination of the differences between the optimized $(CNH_2)_2Pt_2$ and $(CND_2)_2Pt_2$ force constants for similar internal coordinates shows that although the values are generally very similar, there are a few notable exceptions. The DND and DNC bend and the ND–CN and CC–CN stretch–stretch interaction force constants are somewhat larger than the corresponding hydrogenated values, while under the harmonic approximation they should be the same. Since the observed frequencies were used directly without correcting for anharmonicity, the resulting optimized harmonic force constants are likely to be somewhat erroneous, especially for the DND and related DNC bend modes, which are known to be highly anharmonic [45]. Furthermore, coupling constants excluded from the calculations, such as the HNH–CN bend–stretch interaction, may not be negligible as was assumed.

4.3. The characterization of aminomethylidyne dimers

Spectra assigned to aminomethylidyne dimers are observed both from HCN exposures of 0.2–0.8 L (Fig. 4A) and from the thermal decomposition of diaminoethylene (Fig. 4B). A detailed description of the evolution of the spectra of Fig. 4A from isolated aminomethylidyne units to large hydrogen-bonded aggregates is described elsewhere [22], as is a complete description of the thermal chemistry of cyanogen and hydrogen on Pt(111) [25]. Here we focus on the spectra of the small aggregates which are common to Fig. 4A and B with bands at 1347, 1574, 3262–3263, and 3441 cm^{-1}. These bands are seen in Fig. 4A for HCN exposures of 0.2–0.4 L and for the 400 K anneal of Fig. 4B, which mainly yields isolated aminomethylidyne as revealed by the more intense bands at 1328, 1566, and 3368 cm^{-1}. Spectra attributed to aminomethylidyne aggregates are also observed following azomethane, $CH_3N_2CH_3$, thermal decomposition on Pt(111) [19].

To gain further insight into the species responsible for the bands at 3441, 3263, 1574,

and 1347 cm^{-1} a normal mode analysis based on a $(CNH_2)(CNH_2)Pt_3$ 'aminomethylidyne dimer' model was performed. A number of space filling diagrams, based on the van der Waals radii of the constituent atoms within CNH_2, show that only adsorbates occupying adjacent bridge or 3-fold hollow sites on Pt(111) are in close enough proximity to form a hydrogen bonded dimer. In conjunction with the structure of CNH_2 in $Os_3(\mu\text{-}CNH_2)(CO)_{10}$ [36] and its calculated geometry on Ni(111) [13], it was assumed that the CNH_2 units of an aminomethylidyne dimer would occupy bridge sites. However, these calculations do not exclude the possibility that the CNH_2 units of such species can occupy adjacent 3-fold sites. The low number of observed bands indicates that such a dimer must possess at least C_2 symmetry. This in turn negates the possibility of the dimer possessing a single linear intermolecular hydrogen bond, since the resulting species would have either C_1 or C_s symmetry and give rise to a greater number of bands than are observed experimentally. In order to retain C_2 symmetry, the CNH_2 units of such a system must be perturbed in a symmetric fashion to avoid steric hindrances, while preserving the Van der Waals radii criteria necessary for the formation of intermolecular hydrogen bonds. Of the possible geometric models considered, it is shown that a structure with a pair of planar CNH_2 units tilted by $+$ and -18 degrees relative to the surface normal satisfies both of these requirements [29]. Since the dimer retains two fold symmetry, it is likely that a pair of cooperative $N{-}H\cdot\cdot\pi$ hydrogen bonds are formed, such as observed for pyrazole dimers [46] and a number of similar systems [47–49]. For analogous systems, such as benzophenone (4-nitrophenyl) hydrozone [47], the N–H coordinate of the sp^2 hybridized N atom is shown to form a strong hydrogen bond with the π_{C-C} orbital on an adjacent phenyl ring. The resulting $N{-}H\cdot\pi$ hydrogen bond has an angle of 113° while the N=N–H and phenyl planes make a dihedral angle of 52°, giving an effective tilt angle of 26°. These values are similar to the analogous coordinates derived for the CNH_2 dimer, which is calculated to have similar bend and tilt angles of 106° and 18°. Based on these findings, a $(CNH_2)(CNH_2)Pt_3$ geometric model representing the most likely structure that an aminomethylidyne dimer would adopt on Pt(111), as shown in Fig. 5, was constructed.

A total of 27 force constants, 15 unique, were used throughout the calculations. Since each of the CNH_2 moieties of the dimer model are in many ways similar to those of the monomer, in that they are tilted by only $\pm 18°$ with respect to the surface normal while remaining planar, analogous optimized force constants derived from the $(CNH_2)Pt_2$ calculation were used as initial force constants for the nonhydrogen bonded coordinates of the $(CNH_2)(CNH_2)Pt_3$ model. Force constants of 0.300 mdyn $Å^{-1}$ and 0.026 mdyn Å rad^{-2} were assigned [22] and estimated for the corresponding $N\cdot\cdot H$ stretch and $N{-}H\cdot\cdot N$ bend coordinates of each 'new' hydrogen bond created. The initial force constants of the NH stretch, HNC bend and CN stretch coordinates of each CNH_2 unit, perturbed by the formation of a pair of hydrogen bonds, were systematically altered by up to -10%, $+10\%$, and $+10\%$ in order to determine by what degree these values should be modified in order to effectively model the observed spectra. The best set of initial force constants obtained in this way are given in Table 3a and had an RMS error of 50 cm^{-1}. The difference between this set and those of the aminomethylidyne monomer are consistent with the results of a number of complementary studies [50,51]. For example, similar trends among the force constants of *N*-methylacetamide were calculated for its formation of a hydrogen bond with water [50]. The fact that the experimental data was well modeled by merely assigning reasonable values to the force constants of internal coordinates either created or perturbed by the formation of a pair of hydrogen bonds validates the dimer model. This also indicates that although the number of unique force constants

Table 6
Experimental and calculated frequencies (cm^{-1}) for the aminomethylidyne dimer

Isotopomer[12]		$\nu(NH)_s$	$\nu(NH)_s^a$	$\delta(NH_2)^a$	$\nu(CN)^a$
$C^{14}NH_2$	Expt.	3441	3262	1574	1347
	Calc.	3442	3363	1580	1279
$^{12}C^{15}NH_2$	Expt.	3431	3256	1565	1335
	Calc.	3433	3256	1571	1277
$^{13}C^{14}NH_2$	Expt.	3441	3262	1574	1313
	Calc.	3442	3263	1569	1362

[a] Normal modes due to hydrogen-bonded internal coordinates.

exceeds the observed number of bands by three, a reliable set of force constants can still be obtained upon final optimization. Also, force constants associated with inconsequential internal coordinates, such as Pt–Pt stretches and Pt–Pt–Pt bends, were included in the optimization procedure, even though it is evident that their exclusion would have had a negligible effect on the final result.

Having established a reliable set of initial force constants, these values were fitted to the experimental frequencies. The best fit force constants calculated for the $(CNH_2)(CNH_2)Pt_3$ model, displayed in Table 3b, only differ from their initial values by an average of $\pm 1.43\%$, while yielding an RMS error in frequency between calculated and observed values of only 30 cm^{-1}. It can be seen that the best fit frequencies generated by the model, displayed in Table 6, are in close agreement with those observed experimentally. These normal mode calculations using a $(CNH_2)(CNH_2)Pt_3$ model further support the assignment of the common spectral features seen during (CNH_2) aggregation [22] as well as $CH_3N_2CH_3$ [19] and $(CNH_2)_2$ [25] thermal decomposition on Pt(111) to a hydrogen bonded aminomethylidyne dimer.

5. Summary

(1) Normal mode calculations based on $(CNH_2)Pt_2$ and HCNHPt models support assignment of RAIR, spectra obtained from HCN and CH_3NH_2 decomposition [19,20,30], and CN hydrogenation on Pt(111) [21,23,25], to a monomeric aminomethylidyne (CNH_2) species. An independent ab initio study [13] shows that CNH_2 is stable on Ni(111) and has vibrational frequencies similar to those observed on Pt(111). The force constants obtained from this simplest species containing the iminium-like, $-(C{=}NH_2)$, functionality provided good initial force constants for calculations of the two more complicated species described below.

(2) Normal coordinate calculations utilizing two $(CNH_2)_2Pt_2$ models, representing possible olefinic and acetylinic configurations $(CNH_2)_2$ may adopt on Pt(111), demonstrate that μ_2, η^2-diaminoethylene $(H_2NC{=}CNH_2)$, bonding to the surface with a parallel dimetalated olefin configuration, is formed by the reaction of cyanogen and hydrogen on Pt(111) [21,23–25].

(3) A $(CNH_2)(CNH_2)Pt_3$ model shows that the vibrational spectra of the common species observed from CNH_2 aggregation [22], as well as from $CH_3N_2CH_3$ [19] and $(CNH_2)_2$ [25] thermal decomposition on Pt(111), is most likely due to the formation of a hydrogen-bonded aminomethylidyne dimer.

Acknowledgements

This work was funded by a grant from the National Science Foundation (CHE 9616402). The authors thank Prof. Cynthia Jameson for helpful discussions concerning the normal mode calculations.

References

[1] H. Ibach, D.L. Mills, Electron Energy Loss Spectroscopy and Surface Vibrations, Academic Press, New York, 1982.
[2] D.C. Harris, M.D. Bertolucci, Symmetry and Spectroscopy, An Introduction to Vibrational and Electronic Spectroscopy, Dover Publications, New York, 1989.
[3] E. Bright Wilson Jr., J.C. Decius, P.C. Cross, Molecular Vibrations, The Theory of Infrared and Raman Vibrational Spectra, Dover Publications, New York, 1980.

[4] W.J. Orville Thomas, J. Chem. Phys. 20 (1952) 920.
[5] R.E. Dodd, R. Little, Spectrochim. Acta 16 (1960) 1083.
[6] N. Sheppard, Annu. Rev. Phys. Chem. 39 (1988) 589.
[7] E.M. Stuve, R.J. Madix, J. Phys. Chem. 89 (1985) 3183.
[8] H. Celio, M. Trenary, H. Robota, J. Phys. Chem. 99 (1995) 6024.
[9] G. Fogarasi, P. Pulay, Annu. Rev. Phys. Chem. 35 (1984) 191.
[10] G. Fogarasi, P. Pulay, in: J.R. Durig (Ed.), Vibrational Spectra and Structure, Vol. 14, 1985.
[11] J.L. Whitten, Chem. Phys. 117 (1993) 387–397, and references therein.
[12] H.H. Yang, J.L. Whitten, C.M. Friend, Surf. Sci. 313 (1994) 295–307.
[13] H. Yang, J.L. Whitten, Chem. Phys. Lett. 251 (1996) 20–25.
[14] H. Yang, J.L. Whitten, J. Phys. Chem. 100 (1996) 5090–5097.
[15] J.L. Whitten, H. Yang, Surf. Sci. Rep. 24 (1996) 55–124, and references therein.
[16] W.S. Sim, D.A. King, J. Phys. Chem. 100 (1996) 14794.
[17] P. Skinner, M.W. Howard, I.A. Oxton, S.F.A. Kettle, D.B. Powell, N. Sheppard, J. Chem. Soc., Faraday Trans. 77 (1981) 1203.
[18] M.D. Weisel, J.G. Chen, F.M. Hoffmann, Y.-K. Sun, W.H. Weinberg, J. Chem. Phys. 97 (1992) 9396.
[19] D. Jentz, M. Trenary, X. Peng, P. Stair, Surf. Sci. 341 (1995) 282–294.
[20] D. Jentz, H. Celio, P. Mills, M. Trenary, Surf. Sci. 341 (1995) 1–8.
[21] D. Jentz, P. Mills, H. Celio, M. Trenary, Surf. Sci. 368 (1996) 354.
[22] D. Jentz, P. Mills, H. Celio, M. Belyansky, M. Trenary, J. Chem. Phys. 105 (8) (1996) 3250–3257, and references therein.
[23] P. Mills, D. Jentz, H. Celio, M. Trenary, J. Am. Chem. Soc. 118 (1996) 6524–6525.
[24] P. Mills, D. Jentz, M. Trenary, Surf. Sci. 368 (1996) 348, and references therein.
[25] P. Mills, D. Jentz, M. Trenary, J. Am. Chem. Soc. 119 (1997) 9002.
[26] M.E. Brubaker, M. Trenary, J. Chem. Phys. 85 (1986) 6100.
[27] P.L. Hagens, I. Chorkendorff, J.T. Yates Jr., J. Chem. Phys. 92 (1988) 471.
[28] QCPE Program No. QCMP 067, D.F. McIntosh, M.R. Peterson, Quantum Chemistry Program Exchange, Indiana University, Dept. of Chem., 1988.
[29] P. Mills, PhD Thesis, University of Illinois at Chicago, 1997.
[30] W. Erley, J.C. Hemminger, Surf. Sci. 316 (1994) L1025–L1030.
[31] D.M. Hoffman, R. Hoffmann, C.R. Fisel, J. Am. Chem. Soc. 104 (1982) 3858.
[32] F.A. Cotton, G. Wilkinson, Advanced Inorganic Chemistry, 5th edn., Wiley-Interscience, 1988.
[33] P. Botschwina, Chem. Phys. Lett. 29 (1974) 580.
[34] M.E. Kordesch, W. Stenzel, H. Conrad, Surf. Sci. 205 (1988) 100–116.
[35] J.G. Serafin, C.M. Friend, J. Phys. Chem. 92 (1988) 6694.
[36] A.J. Deeming, S. Donovan-Mtunzi, S.E. Kabir, J. Chem. Soc., Dalton Trans. (1987) 1457.
[37] M.R. Churchill, B.G. Deboer, F.J. Rotella, E.W. Abel, R.J. Rowley, J. Am. Chem. Soc. 97 (1975) 7158.
[38] M.R. Churchill, B.G. Deboer, F.J. Rotella, Inorg. Chem. 15 (1976) 1843.
[39] M.A. Andrews, G. Van Burskirk, C.B. Knobler, H.D. Kaesz, J. Am. Chem. Soc. 101 (1979) 7245–7253.
[40] B.N. Storhoff, H.C. Lewis, Coordination Chem. Rev. 23 (1977) 1–29, and references therein.
[41] E. Parmeter, M.M. Hills, W.H. Weinberg, J. Am. Chem. Soc. 108 (1986) 3563.
[42] L.L. Kesmodel, R.C. Baetzold, G.A. Somorjai, Surf. Sci. 66 (1977) 299.
[43] J.A. Gates, L.L. Kesmodel, J. Chem. Phys. 76 (1982) 4281.
[44] A. Fadini, F.M. Schnepel, Vibrational Spectroscopy, Methods and Applications, Ellis Horwood, Chichester, 1989.
[45] A.Y. Hirakawa, M. Tsuboi, T. Shimanouchi, J. Chem. Phys. 57 (1972) 1236.
[46] C. Hamilton, J. Ibers, Hydrogen Bonding in Solids: Methods of Molecular Structure Determination, Benjamin, New York, 1968.
[47] M.G.B. Drew, G.R. Willey, J. Chem. Soc., Perkin Trans. 2 (1986) 215.
[48] J. Masnovi, R.J. Baker, R.L.R. Towns, Z. Chen, J. Org. Chem. 56 (1991) 176–179.
[49] Rodham et al., Nature 362 (1993) 735.
[50] M.G. Mirkin, S. Krimm, J. Am. Chem. Soc. 113 (1991) 9742–9747.
[51] J.J. Lopez-Garriga, S. Hanton, G.T. Babcock, J.F. Harison, J. Am. Chem. Soc. 108 (1986) 7251–7254.